European Journal of Radiology 118 (2019) 32–37

Contents lists available at ScienceDirect

European Journal of Radiology

journal homepage: www.elsevier.com/locate/ejrad

Research article

Machine learning-based radiomics strategy for prediction of cell proliferation in non-small cell lung cancer

Qianbiao Gu[a,b], Zhichao Feng[a], Qi Liang[a], Meijiao Li[a], Jiao Deng[a], Mengtian Ma[a], Wei Wang[a], Jianbin Liu[b], Peng Liu[b], Pengfei Rong[a,*]

[a] Department of Radiology, The Third Xiangya Hospital of Central South University, Changsha 410013, China
[b] Department of Radiology, The People's Hospital of Hunan Province, The First Hospital Affiliated of Hunan Normal University, Changsha 410005, China

ARTICLE INFO

Keywords:
Non-small cell lung cancer (NSCLC)
Ki-67
CT
Radiomics
Machine learning

ABSTRACT

Purpose: To explore the feasibility and performance of machine learning-based radiomics classifier to predict the cell proliferation(Ki-67)in non-small cell lung cancer (NSCLC).

Methods: 245 histopathological confirmed NSCLC patients who underwent CT scans were retrospectively included. The Ki-67 proliferation index (Ki-67 PI) were measured within 2 weeks after CT scans. A lesion volume of interest (VOI) was manually delineated and radiomics features were extracted by MaZda software from CT images. A random forest feature selection algorithm (RFFS) was used to reduce features. Six kinds of machine learning methods were used to establish radiomics classifiers, subjective imaging feature classifiers and combined classifiers, respectively. The performance of these classifiers was evaluated by the receiver operating characteristic curve (ROC) and compared with Delong test.

Results: 103 radiomics features were extracted and 20 optimal features were selected using RFFS. Among the radiomics classifiers established by six machine learning methods, random forest-based radiomics classifier achieved the best performance (AUC = 0.776) in predicting the Ki-67 expression level with sensitivity and specificity of 0.726 and 0.661, which was better than that of subjective imaging classifiers (AUC = 0.625, $P < 0.05$). However, the combined classifiers did not improve the predictive performance (AUC = 0.780, $P > 0.05$), with sensitivity and specificity of 0.752 and 0.633.

Conclusions: The machine learning-based CT radiomics classifier in NSCLC can facilitate the prediction of the expression level of Ki-67 and provide a novel non-invasive strategy for assessing the cell proliferation.

1. Introduction

Lung cancer is the leading cause of cancer-related deaths worldwide [1,2]. Currently, more and more treatment methods can be used for treatment of lung cancer. However, many patients, even patients with resectable lung cancer, still have a poor prognosis [3]. One of the reasons may be that cancers are spatially and temporally heterogeneous [4]. Therefore, there is an urgent need for more convenient and appropriate bio-markers to dynamically monitor the characteristics of tumour biological behaviour.

Ki-67 nucleoprotein (also known as MKi-67) is a key marker that is associated with cell proliferation and tumour heterogeneity. Its expression levels increase from G1 to mitosis and then decrease rapidly, but does not exist in quiescent cells (G0 phase).So, Ki-67 has been used to distinguish growing and non-growing cells [5–7]. In a cohort study of 109 NSCLC patients, the median disease-free survival (DFS) decreased as the expression of Ki-67 increased [8]. Therefore, predicting the Ki-67 expression level accurately is important for monitoring tumour aggressiveness.

However, the Ki-67 expression level can only be determined by post-operative specimens and the accuracy of pre-operative fine-needle aspiration biopsy to determine Ki-67 proliferation index (Ki-67 PI) expression levels is still challenging in clinical practice. What's more, those methods are not only invasive, but also may cause bleeding, pneumothorax and increase the possibility of tumour metastasis [9]. In theory, the histopathological changes caused by expression of genes and cytokines can be directly or indirectly reflected by imaging techniques. Radiomics features can be used to quantify image pixels and the grey-scale spatial distribution, which reflect the corresponding molecular pathological changes at the micro level [10,11].

Several previous studies have found that MRI texture features could be used to predict the Ki-67 expression level in thyroid cancer [12],

* Corresponding author.
E-mail address: rongpengfei66@163.com (P. Rong).

https://doi.org/10.1016/j.ejrad.2019.06.025
Received 6 January 2019; Received in revised form 22 June 2019; Accepted 26 June 2019

breast cancer [13], liver cancer [14], and glioma [15]. Zhou Bodong et al. [16] found that twelve contrast CT radiomic features were significantly associated with tumor Ki-67 status in patients with lung cancer. However, they did not build a predictive model, besides non-enhanced CT scan is the most commonly used for lung cancer patients. Therefore, the feasibility and value of machine learning-based non-enhanced CT radiomics strategy for predicting the Ki-67 expression level in NSCLC have not been validated. The goal of this study is to develop machine learning-based non-enhanced CT radiomics classifiers to noninvasively predict the expression level of Ki-67 in NSCLC and to evaluate the increment compared with the subjective imaging features classifiers.

2. Materials and methods

2.1. Patients

NSCLC patients treated at our institute from January 2014 to March 2018 were retrospectively enrolled in this study under institutional ethics committee approval, and informed consent was waived. The inclusion criteria were as follows: (1) patients with disease confirmed by histopathological examination who had Ki-67 proliferation index (Ki-67 PI) expression levels measured; (2) those who underwent lung three-dimensional CT examination within two weeks before histopathological examination at our institute; and (3)those who did not receive anti-tumour therapy (radiation therapy, chemotherapy or other treatment, etc.) before CT examination. The exclusion criteria were as follows: (1) patients with other concurrent primary malignant tumours and (2) those with CT images with an unclear lung mass tha did not meet the requirements for image post-processing.

A total of 245 patients were included in the study including 176 males and 69 females aged 31–85 years (mean age, 59 years). Of the 245 patients, 149 had adenocarcinoma, and 96 had squamous cell carcinoma.

2.2. CT image acquisition

All patients were scanned using 5 mm CT slice thickness. Of the 245 patients scanned, 153 were scanned with a Brilliance 64 scanner (Philips Brilliance 64; Philips Healthcare, Best, the Netherlands), 55 were scanned with a GE revolution 256 scanner, (GE revolution 256; GE Healthcare, Wis, the Milwaukee) and 37 were scanned with a Somatom Emotion 6 scanner (Somatom Emotion 6; Siemens AG, Erlangen, the Germany), with tube voltages of 120–140 kV and tube currents of 200–210 mA, a pitch of 5 mm and a FOV of 350 × 350 mm. The patient was placed in a supine position with both hands on both sides of the head and breath-hold scans were performed.The scan ranged from above the apex of the lungs to below the level of the diaphragm.

2.3. Immunohistochemical analysis

All specimens were surgically resected tumours of were obtained from needle biopsies (two or three reliable tumour tissue samples) to ensure that the Ki-67 detection represented the entire tumour. A ready-to-use immunohistochemistry EliVision Plus kit((Maixin, Fuzhou, China) was used. The primary antibodies were a mouse anti-human Ki-67 antigen immunohistochemistry monoclonal antibody. The antigen-antibody reaction experiment was performed by referring to the kit instructions. According to 50-fold microscopy, in each section, 1000 cells were randomly selected, and the positive cells were counted. The cut-off point for high Ki-67 PI expression was considered when ≧50% positive cells were observed [17,18]. Samples were classified into two groups: high Ki-67 PI expression (Ki-67≧50%) and low Ki-67 PI expression (Ki-67 < 50%).

2.4. Subjective imaging feature evaluation

According to the lung cancer related research literature [19–21],we defined six clinically subjective imaging features including the lobulation sign, spicule sign, cavitation, cystic necrosis, pleural indentation, and pleural effusion to compare with radiomics features. (Two diagnostic radiologists with 3 and 9 years of experience reviewed the CT images of each patient and identified positive and negative findings by consensus; the entire process was performed without knowledge of the patient's pathological results). A lobulation sign was one with at least three relatively obvious undulations in the margin of the mass; Spicule sign was defined as the presence of relatively sharp linear projections in the interface between the mass and the lung parenchyma; Cavitation was interpreted as the presence of one or more at least 5-mm round or roundish forms of air attenuation in the lesion; Cystic necrosis was the presence of water-like density in the lesion; Pleural indentation was defined as the increased linear or curtain density between tumor and pleura; Pleural effusion was a common clinical symptom characterized by the accumulation of pathological fluid in the pleural cavity.

2.5. Tumour segmentation

Of the 245 patients scanned, 200 patients received contrast and non-contrast CT scan, and 45 patients only received non-contrast CT scan. The non-contrast CT scan images of all patients were exported in DICOM format from the PACS system workstations and then imported into the texture analysis software MaZda (version 4.7, The Technical University of Lodz, Institute of Electronics, http://www.eletel.p.lodz.pl/mazda/). To obtain the volume of interest (VOI) for further radiomic analysis, first the tumour was found in 3D view mode, then, the tumour of interest was drawn in 2D edit mode, and finally 3D tumour segmentation was completed. (Two diagnostic radiologists with 3 and 9 years of experience finished this by consensus; the entire operation was performed without knowledge of the patient's pathological results).

2.6. CT image feature extraction

MaZda software was used to analyse the manually drawn VOI. For each VOI, before the texture feature extraction, grey-level normalization was performed using the limitation of dynamics to $\mu \pm 3\delta$ (μ - grey level mean, δ - standard deviation) to minimize the influence of contrast and brightness variation, as described previously in similar investigations [22]. At last, 103 radiomics features were extracted. The radiomics features extracted by MaZda include (1) greyscale histogram features (mean, variance, skewness coefficient, kurtosis, and first, 10th, 50th, 90th, and 99th percentiles); (2) absolute gradients (gradient mean, variance, skewness coefficient, kurtosis and non-null); (3) run-length matrix (run-length inhomogeneity, grey inhomogeneity, long run weight, short run weight and run-length image score); and (4) co-occurrence matrix (entropy, contrast, autocorrelation, sum of squares, mean and variance, entropy, variance, difference entropy and deficit moment).

2.7. Feature selection and predictive classifier establishment

A feature selection algorithm based on random forest (RFFS) methods was adopted. This algorithm adopts a random forest algorithm as the basic tool using the classification accuracy as the criterion and then adopts the 10-fold cross validation method and the sequential backward selection method to select features. Each time, one feature that was the least important (had the minimum importance score) was removed from the feature set followed by successive iterations, and the classification accuracy was calculated. Finally, a set of texture features with the least number of variables and relatively high classification accuracy were obtained as the optimal feature subset. All processes were performed on the R 3.4.3 platform (R Foundation for Statistical

Computing, Vienna, Austria URL https://www.R-project.org/).

Machine learning has became the mainstream method of Radiomic research. It could lead to a better discriminant power than classical statistics when analyzing several tens of features [23–25].The R Caret package (version 6.0–47) was used to establish the classifiers. This package provided a comprehensive, good interface to access many machine learning algorithms in R, which included "glm" (L2-LOG), "MASS" (LDA), "caret" (CART), "kNN" (KNN), "e1071" (SVM), and "randomForest" (RF). We used 10-fold cross-validation and repeated the method 50 times to evaluate the classifier and then used the average area under the receiver operating characteristic (ROC) curve (AUC) to represent and compare classifiers. We studied three types of classifiers, including radiomics classifiers, subjective imaging feature classifiers and combined classifiers. Among them, the radiomics classifier only contained 20 radiomics features. The subjective imaging features classifier contained six clinically subjective imaging features, and the combined classifier was a predictive model that integrated six clinically subjective imaging features and 20 radiomics features. In addition, each type of classifier used six kinds of machine learning methods including two-category logistic regression (L2-LOG), linear discriminant analysis (LDA), classification tree and regression tree (CART), K-neighbour clustering (KNN), radial support vector machine (SVM), and random forest (RF). This combination included simple linear mixing (LDA, L2-LOG), nonlinear (CART, KNN) and complex nonlinear methods (SVM, RF). We re-set random numbers before running to ensure that each algorithm's evaluation was run using the same data splitting conditions, which ensures that all the results were comparable (Fig. 1).

2.8. Statistical analysis

SPSS 20.0 (IBM, Armonk, NY, USA) statistical analysis software was used to perform the $\chi 2$ test or *t*-test for the basic clinical data of patients. The difference was statistically significant at $P < 0.05$. A receiver operating characteristic curve (ROC) was used to evaluate the diagnostic performance of different classifiers.

3. Results

3.1. Differences in Ki-67 based on sex, age, and pathology

According to the expression level of the Ki-67 PI, patients were divided into two groups; 117 patients had high Ki-67 PI expression, and 128 patients had low Ki-67 PI expression. Univariate analysis of gender, age, pathological type and the expression level of Ki-67 PI revealed that gender, age, and pathological type were significantly different between the high and low Ki-67 PI expression groups. The differences were statistically significant (all *P* values were < 0.05). It seems that high Ki-67 PI expression was more common in men, older patients and squamous cell carcinoma patients (see Table 1).

Table 1
Basic clinical data of the two groups of patients with non-small cell lung cancer.

Clinical characters	High Ki-67 PI expression group	Low Ki-67 PI expression group	*P*
Total (patients)	117	128	
Age	60 (48-85)	57 (31-79)	0.007
Gender			0.000
Male	93 (79%)	83 (65%)	
Female	24 (21%)	45 (35%)	
Histopathological type			0.000
Adenocarcinoma	47 (40%)	102 (80%)	
Squamous cell carcinoma	70 (60%)	26 (20%)	

() Internal measurement data indicate percentage, count data indicate range.Ki-67 PI: Ki-67 proliferation index.

3.2. Selection of texture features

At last, 103 radiomics features were extracted from MaZda software. A wrapper-based feature selection method (RFFS) was performed to reduce radiomics features. In total, 20 radiomics features were selected as the optimal radiomics feature subset based on the relationship between the classification accuracy and the number of features for the radiomics classifier (see Fig. 2). These features include 5 histogram features, 10 co-occurrence matrix features, and 5 run-length matrix features.

3.3. Establishment of predictive classifiers and comparison

We first explored whether the image features could distinguish between the high Ki-67 PI expression group and the low Ki-67 PI expression group. The results showed that each feature of the 20 texture features could discriminate the two groups with an average AUC ranging from 0.52 to 0.67, and the feature with the best performance was Vertl-GLevNonU (with an AUC of 0.67, 95% confidence interval 0.60˜0.74). Each subjective imaging feature could be used to discriminate the two groups with an average AUC ranging from 0.51 to 0.57, and the feature with the best performance was liquefaction necrosis (with an AUC of 0.57, 95% confidence interval 0.50˜0.65) (Table 2). The high Ki-67 PI expression group was more inclined to have liquefaction necrosis than the low Ki-67 PI group (Fig. 3) (Table 2).

Then, we used each set of features to build multivariate predictive classifier, including the subjective imaging feature classifier (6 subjective imaging features), radiomics classifier (20 texture features), and combined prediction classifier (26 features). Each classifier used 6 kinds of machine learning methods. The results showed the RF method

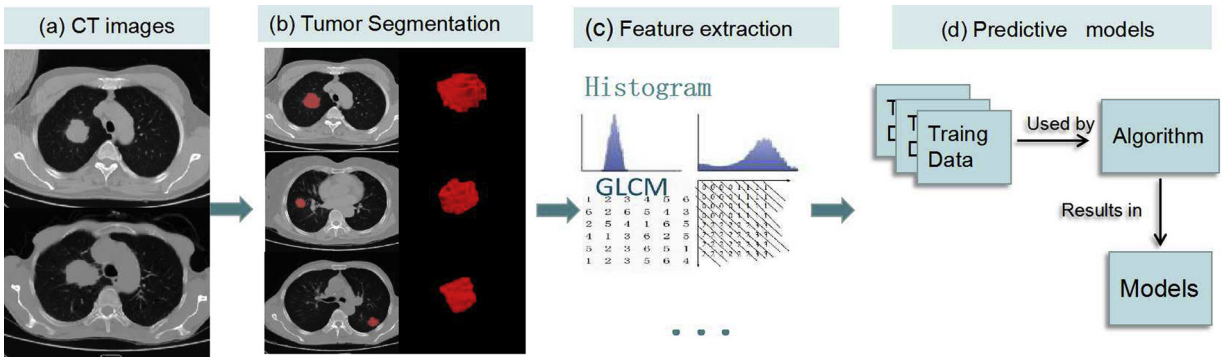

Fig. 1. Workflow of radiomics analysis to predict the Ki-67 expression level in patients with NSCLC. Acquiring CT images and experienced radiologists delineate the volume of interest (VOI) (a,b). Radiomics features are extracted from the VOI on non-enhanced CT images (c). A random forest feature selection algorithm (RFFS) was used to reduce features And six kinds of machine learning methods were used to establish predictive classifiers (d).

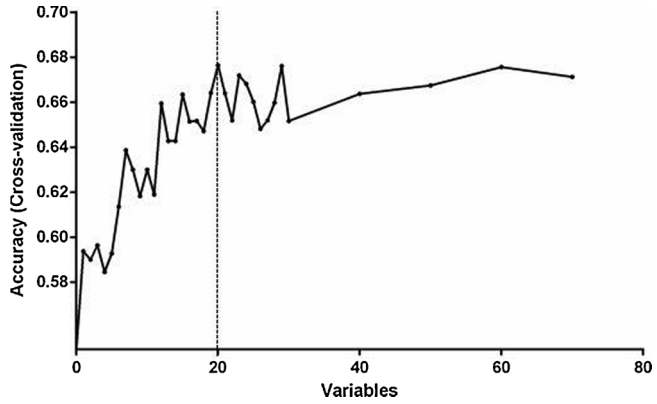

Fig. 2. Relationship between classification accuracy and feature number. The dotted lines represent the number of features when the model had the best predictive ability.

Table 2
Comparison of subjective imaging features in high Ki-67 PI expression group and low Ki-67 PI expression group.

Subjective imaging features	High Ki-67 PI expression	Low Ki-67 PI expression	AUC
lobulation sign			0.543
yes	96	94	
no	21	34	
spicule sign			0.540
yes	39	53	
no	78	75	
cavitation			0.524
yes	12	7	
no	105	121	
cystic necrosis			0.573
yes	18	1	
no	99	127	
pleural indentation			0.538
yes	24	36	
no	93	92	
pleural effusion			0.513
yes	7	11	
no	110	117	
gender			0.573
male	93	83	
female	24	45	
age	60	57	0.596

Note: AUC: area under curve; Ki-67 PI: Ki-67 proliferation index.

among machine learning methods achieved the best result, The highest average AUC for the subjective imaging feature classifier, radiomics classifier, and combined prediction classifier was 0.625, 0.776, and 0.782, respectively. The sensitivity was 0.780, 0.776, 0.752 and the specificity was 0.417, 0.661, 0.633, respectively. The radiomics classifier and the combined prediction classifier showed significantly better performance than the subjective imaging feature classifier (AUC: 0.776 vs. 0.625; 0.782 vs. 0.625; $P < 0.05$). However, compared with the radiomics classifier, even with the addition of the subjective imaging features, the performance of the combined prediction classifier did not improve (Fig. 4).

3.4. Stratified analysis for radiomics signature by gender and tumour histopathological type

Furthermore, stratified analysis showed that the radiomics classifier was still an independent predictor for determining Ki-67 PI expression levels even after adjusting for gender and tumour histopathological type. The average AUC was 0.80 for males, 0.72 for females, 0.79 for adenocarcinoma, and 0.76 for squamous cell carcinoma. These analyses showed that the radiomics classifier exhibited good performance for predicting Ki-67 PI expression even in NSCLC patients in the subgroups, especially in male adenocarcinoma patients.

4. Discussion

In this study, a machine learning-based CT radiomics classifier was built as a noninvasive predictor of Ki-67 PI expression levels in patients with NSCLC. Furthermore, in the subgroup stratified by gender, the radiomics classifier was also shown to be a useful satisfactory predictor. To our knowledge, this is the first study to establish a radiomics classifier using CT images to predict Ki-67 PI expression levels. The analysis revealed that the radiomics classifier could classify a patient's Ki-67 PI status with good performance.

Our results showed that high Ki-67 PI expression was more common in men, older patients, and squamous cell carcinoma patients. Previous studies have found that the women with adenocarcinoma who were receiving chemotherapy or surgical treatment had a better prognosis than men with squamous cell carcinoma [26,27]. The abovementioned findings indirectly confirmed that the Ki-67 PI plays an important role in predicting the prognosis of NSCLC.

The study found that the radiomics classifier can predict Ki-67 PI expression levels in patients with NSCLC, with an AUC of 0.77. Radiomics is a rapidly growing field that enables high-throughput automated analysis of quantitative image data. There are several radiomics studies where Ki-67 PI prediction was evaluated. Meyer et al [12] explored the correlations between MRI radiomics features and Ki-67 PI expression in thyroid cancer. Liang C et al [13] found that a T2W image-based radiomics classifier was a significant predictor of Ki-67 PI status in patients with breast cancer. Compared to these studies, our study used CT images, which is more commonly used in clinical practice. Ganeshan et al [27] found that the texture features of NSCLC on CT were significantly correlated with the expression of tumour glucose transporter 1 (Glut-1) and tumour CD34, indicating that the CT radiomics features of the lesion reflected tumour angiogenesis and histopathological changes, such as hypoxia. However, those markers indirectly reflect tumour proliferation. In our study, machine learning-aided radiomics approaches were applied to detect the Ki-67 PI, which can directly reflect tumour proliferation. As several previous studies have confirmed, a variety of tumours with different expression levels of Ki-67 proliferation index have significant differences in cell proliferation, cell differentiation, and composition of subcloning regions [28–30]. Those differences are implied in clinical medical images, and representative changes in image texture features, such as pixel value, greyscale, and complexity, are beyond detectability by human eyes [31]. Thus, we used CT image texture features to build a radiomics model for predicting the Ki-67 PI in NSCLC patients and obtained good results. Our primary experiments have proved the feasibility of predicting tumour immunohistochemical markers based on conventional CT images of patients with NSCLC and elucidated further information about tumour proliferation and relevant biological behaviour.

In comparison, the performance of the radiomics classifier was better than that of the subjective image feature classifier for predicting Ki-67 PI expression levels. In addition, the average AUC of the best single texture feature (GLevNonU) was higher than that of the best single subjective image feature (liquefaction necrosis); the AUC was 0.67 vs. 0.57, respectively. GLevNonU (grey-level non-uniformity) is a measure of the homogeneity of the pixel grey level distribution of the underlying tissue, where higher values represent more inhomogeneity within the grey levels of the run-length matrix [32]. Hence, the superiority of GLevNonU in differentiating Ki-67 PI expression level shows that high cell proliferation might be associated with a more heterogeneous tissue texture. Regarding liquefaction necrosis, it is thought to be caused by chronic ischaemia within tumours and by rapid tumour cell growth overtaking the rate of neovascularization in a given area [33]. Hence, the high Ki-67 PI expression group was more prone to

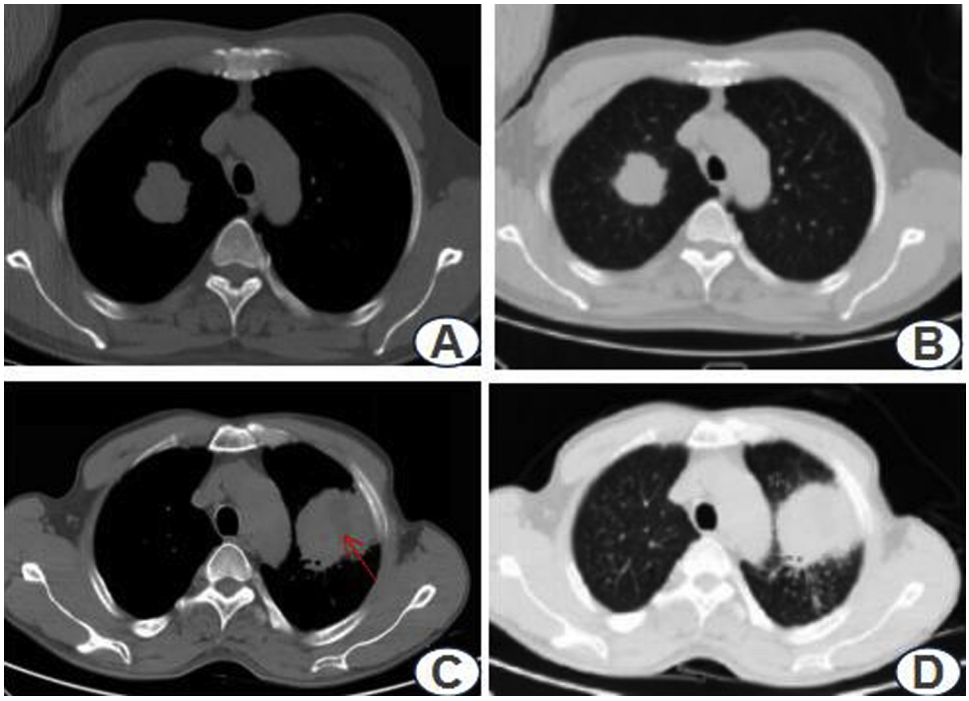

Fig. 3. A 49-year-old male patient with low Ki-67 expression (A,B); A 55-year-old male patient with high Ki-67 expression (C,D). Tumours with high Ki-67 expression were more inclined to have liquefaction necrosis than those with low Ki-67 expression (arrow).'.

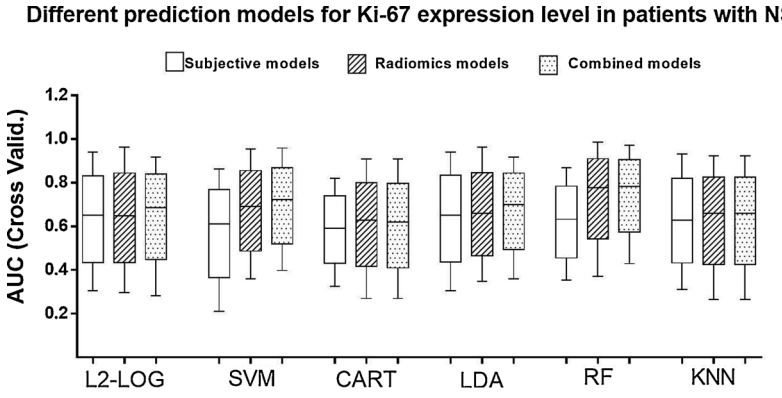

Fig. 4. Different prediction models for Ki-67 expression levels in patients with NSCLC. Six kinds of machine learning methods including L2-LOG:two-category logistic regression (L2-LOG)L2-Logistic Regression, support Vector Machine (SVM), classification tree and regression tree (CART), linear discriminant analysis (LDA), random forest (RF) and K-neighbour clustering (KNN) were used to develop subjective models, radiomics models and combined models.

have liquefaction necrosis. Traditionally, subjective image features are identified when medical images are treated as pictures intended solely for visual interpretation; these features may suffer from large intra and inter-observer variability and may not capture sufficient information, while advanced radiomic features can capture more information. Radiomics data contain multiple-order statistics and can be combined with other patient data and be mined with sophisticated bioinformatics tools to develop models that may potentially improve diagnostic and predictive accuracy [31]. Therefore, our study found that the radiomics classifier was more predictive than the subjective image feature classifier for predicting Ki-67 PI expression levels. There are many studies that have also shown the same results [34–36].

In addition, in the different types of machine learning classifiers established in this study, different classifiers showed different predictive performances, and the average AUC ranged from 0.65 to 0.83, indicating that the choice of the classifier model type had a great influence on the results. Among them, the random forest classifier was superior to other types of classifiers in terms of AUC, specificity and sensitivity. From the perspective of methodology, RF is a set of decision trees. The mechanisms of decision trees can be compensated using different features, and multiple weak tree classifiers can be combined into strong classifiers. Therefore, a set of decision trees can produce good classification results based on even weak feature sets. We found that some other method comparison studies [24,37] have also showed that the RF method outperformed other classifiers. Our results are consistent with these findings.

At last, this study used manual segmentation, It is often regarded as a gold standard. However, it maybe suffered from significant inter-reader bias and time-consuming. In our study, we finished the segmentation by two radiologists' negotiation. According to the size of the tumour, the time spent on each patient was about 1–3 min throughout the whole process. Automatic segmentation is fast, but the accuracy and reproducibility should be considered and need further study.

Our study has several limitations. First, the sample size is small, and the results need to be confirmed with large sample studies. The classifier built in this study was validated with internal data but not tested with external test data. So, in the future, multi-center and large sample studies are encouraged. Second, in this study, squamous cell carcinoma and adenocarcinoma types of NSCLC were studied, but no rare pathological types were included. Finally, the samples were obtained with different types of equipment. Although the images are processed uniformly, the equipment type may still have a certain degree of influence

on the results.

In conclusion, this study shows that the machine learning-based CT radiomics classifier in NSCLC can facilitate the prediction of the expression level of Ki-67 and provide a novel non-invasive strategy for assessing the cell proliferation

References

[1] R. Siegel, K. Miller, A. Jemal, Cancer statistics, 2018, CA Cancer J. Clin. 68 (2018) 7–30.

[2] H. Zeng, W. Chen, R. Zheng, S. Zhang, J. Ji, X. Zou, C. Xia, K. Sun, Z. Yang, H. Li, N. Wang, R. Han, S. Liu, H. Li, H. Mu, Y. He, Y. Xu, Z. Fu, Y. Zhou, J. Jiang, Y. Yang, J. Chen, K. Wei, D. Fan, J. Wang, F. Fu, D. Zhao, G. Song, J. Chen, C. Jiang, X. Zhou, X. Gu, F. Jin, Q. Li, Y. Li, T. Wu, C. Yan, J. Dong, Z. Hua, P. Baade, F. Bray, A. Jemal, X. Yu, J. He, Changing cancer survival in China during 2003-15: a pooled analysis of 17 population-based cancer registries, Lancet Glob. Health 6 (2018) e555–e567.

[3] M. Jamal-Hanjani, S. Quezada, J. Larkin, C. Swanton, Translational implications of tumor heterogeneity, Clin. Cancer Res. 21 (2015) 1258–1266.

[4] G. Lee, H. Lee, H. Park, M. Schiebler, E. van Beek, Y. Ohno, J. Seo, A. Leung, Radiomics and its emerging role in lung cancer research, imaging biomarkers and clinical management: State of the art, Eur. J. Radiol. 86 (2017) 297–307.

[5] J. Gerdes, H. Lemke, H. Baisch, H. Wacker, U. Schwab, H. Stein, Cell cycle analysis of a cell proliferation-associated human nuclear antigen defined by the monoclonal antibody Ki-67, J. Immunol. 133 (1984) 1710–1715.

[6] J. Bullwinkel, B. Baron-Lühr, A. Lüdemann, C. Wohlenberg, J. Gerdes, T. Scholzen, Ki-67 protein is associated with ribosomal RNA transcription in quiescent and proliferating cells, J. Cell. Physiol. 206 (2006) 624–635.

[7] R. Rahmanzadeh, G. Hüttmann, J. Gerdes, T. Scholzen, Chromophore-assisted light inactivation of pKi-67 leads to inhibition of ribosomal RNA synthesis, Cell Prolif. 40 (2007) 422–430.

[8] H. Ahn, M. Jung, S. Ha, J. Lee, I. Park, Y. Kim, J. Hong, S. Sym, J. Park, D. Shin, J. Lee, E. Cho, Clinical significance of Ki-67 and p53 expression in curatively resected non-small cell lung cancer, Tumour Biol. 35 (2014) 5735–5740.

[9] R. Takahashi, T. Nakajima, Y. Sakairi, Y. Matsui, T. Iizasa, H. Kimura, A case of pulmonary and chest wall metastasis from rectal cancer, presumable caused by seeding during CT-guided percutaneous needle biopsy, J. Jpn. Assoc. Chest Surg. 24 (2010) 929–933.

[10] C. Tang, B. Hobbs, A. Amer, X. Li, C. Behrens, J. Canales, E. Cuentas, P. Villalobos, D. Fried, J. Chang, D. Hong, J. Welsh, B. Sepesi, L. Court, I. Wistuba, E. Koay, Development of an immune-pathology informed radiomics model for non-small cell lung cancer, Sci. Rep. 8 (2018) 1922.

[11] Lu Chia-Feng, Hsu Fei-Ting, Hsieh Kevin Li-Chun, Kao Yu-Chieh Jill, Cheng Sho-Jen, Hsu Justin Bo-Kai, Tsai Ping-Huei, Chen Ray-Jade, Huang Chao-Ching, Yen Yun, Chen Cheng-Yu, Machine learning-based radiomics for molecular subtyping of gliomas, Clin. Cancer Res. 24 (2018) 4429–4436.

[12] H. Meyer, S. Schob, A. Höhn, A. Surov, MRI texture analysis reflects histopathology parameters in thyroid cancer - a first preliminary study, Transl. Oncol. 10 (2017) 911–916.

[13] C. Liang, Z. Cheng, Y. Huang, L. He, X. Chen, Z. Ma, X. Huang, C. Liang, Z. Liu, An MRI-based radiomics classifier for preoperative prediction of Ki-67 status in breast cancer, Acad. Radiol. 25 (2018) 1111–1117.

[14] X. Hu, Z. Yang, H. Liang, Y. Ding, R. Grimm, C. Fu, H. Liu, X. Yan, Y. Ji, M. Zeng, S. Rao, Whole-tumor MRI histogram analyses of hepatocellular carcinoma: correlations with Ki-67 labeling index, J. Magn. Reson. Imaging 46 (2017) 383–392.

[15] Y. Li, Z. Qian, K. Xu, K. Wang, X. Fan, S. Li, X. Liu, Y. Wang, T. Jiang, Radiomic features predict Ki-67 expression level and survival in lower grade gliomas, J. Neurooncol. 135 (2017) 317–324.

[16] Zhou Bodong, Xu Jie, Tian Ye, Yuan Shuai, Xubin Li, Correlation between radiomic features based on contrast-enhanced computed tomography images and Ki-67 proliferation index in lung cancer: a preliminary study, Thorac. Cancer 9 (2018) 1235–1240.

[17] S. Yan, J. Shun-Chang, C. Li, L. Jie, L. Ya-Li, W. Ling-Xiong, Topoisomerase II alpha expression and the benefit of adjuvant chemotherapy for postoperative patients with non-small cell lung cancer, BMC Cancer 10 (2010) 621.

[18] C.H. Kim, H.S. Lee, J.H. Park, J.H. Choi, S.H. Jang, Y.B. Park, M.G. Lee, I.G. Hyun, K.I. Kim, H.S. Kim, S.W. Cho, W.Y. Lee, E.J. Kim, H. Kim, J.W. Shim, Y.H. Choi, Prognostic role of p53 and Ki-67 immunohistochemical expression in patients with surgically resected lung adenocarcinoma: a retrospective study, J. Thorac. Dis. 7 (2015) 822–833.

[19] S. Rizzo, F. Petrella, V. Buscarino, F. De Maria, S. Raimondi, M. Barberis, C. Fumagalli, G. Spitaleri, C. Rampinelli, F. De Marinis, L. Spaggiari, M. Bellomi, CT radiogenomic characterization of EGFR, K-RAS, and ALK mutations in non-small cell lung cancer, Eur. Radiol. 26 (2016) 32–42.

[20] Z. Cheng, F. Shan, Y. Yang, Y. Shi, Z. Zhang, CT characteristics of non-small cell lung cancer with epidermal growth factor receptor mutation: a systematic review and meta-analysis, BMC Med. Imaging 17 (2017) 5.

[21] X. Qin, X. Gu, Y. Lu, W. Zhou, EGFR-TKI-sensitive mutations in lung carcinomas: are they related to clinical features and CT findings? Cancer Manag. Res. 10 (2018) 4019–4027.

[22] N. Scaglia, J. Chatkin, J. Pinto, M. Tsukazan, M. Wagner, A. Saldanha, Role of gender in the survival of surgical patients with nonsmall cell lung cancer, Ann. Thorac. Med. 8 (2013) 142–147.

[23] B. Zhang, X. He, F. Ouyang, D. Gu, Y. Dong, L. Zhang, X. Mo, W. Huang, J. Tian, S. Zhang, Radiomic machine-learning classifiers for prognostic biomarkers of advanced nasopharyngeal carcinoma, Cancer Lett. (2017) S0304383517303804.

[24] H. Wang, Z. Zhou, Y. Li, Z. Chen, P. Lu, W. Wang, W. Liu, L. Yu, Comparison of machine learning methods for classifying mediastinal lymph node metastasis of non-small cell lung cancer from 18F-FDG PET/CT images, EJNMMI Res. 7 (2017) 11.

[25] D. Paul, R. Su, M. Romain, V. Sébastien, V. Pierre, G. Isabelle, Feature selection for outcome prediction in oesophageal cancer using genetic algorithm and random forest classifier, Comput. Med. Imaging Graph. (2016) S089561111630132X..

[26] J. Brahmer, S. Dahlberg, R. Gray, J. Schiller, M. Perry, A. Sandler, D. Johnson, Sex differences in outcome with bevacizumab therapy: analysis of patients with advanced-stage non-small cell lung cancer treated with or without bevacizumab in combination with paclitaxel and carboplatin in the Eastern Cooperative Oncology Group Trial 4599, J. Thorac. Oncol. 6 (2011) 103–108.

[27] B. Ganeshan, V. Goh, H. Mandeville, Q. Ng, P. Hoskin, K. Miles, Non-small cell lung cancer: histopathologic correlates for texture parameters at CT, Radiology 266 (2013) 326–336.

[28] G. Cattoretti, M. Becker, G. Key, M. Duchrow, C. Schlüter, J. Galle, J. Gerdes, Monoclonal antibodies against recombinant parts of the Ki-67 antigen (MIB 1 and MIB 3) detect proliferating cells in microwave-processed formalin-fixed paraffin sections, J. Pathol. 168 (1992) 357–363.

[29] Y. Xuan, Y. Choi, Y. Shin, M. Kook, S. Chae, S. Park, H. Chae, S. Kim, An immunohistochemical study of the expression of cell-cycle-regulated proteins p53, cyclin D1, RB, p27, Ki67 and MSH2 in gallbladder carcinoma and its precursor lesions, Histol. Histopathol. 20 (2005) 59–66.

[30] C. Swanton, Intratumor heterogeneity: evolution through space and time, Cancer Res. 72 (2012) 4875–4882.

[31] R. Gillies, P. Kinahan, H. Hricak, Radiomics: images are more than pictures, they are data, Radiology 278 (2016) 563–577.

[32] B. Baeßler, M. Mannil, D. Maintz, H. Alkadhi, R. Manka, Texture analysis and machine learning of non-contrast T1-weighted MR images in patients with hypertrophic cardiomyopathy-Preliminary results, Eur. J. Radiol. 102 (2018) 61–67.

[33] Winther-Larsen Anne, Demuth Christina, Fledelius Joan, Madsen Anne Tranberg, Hjorthaug Karin, Meldgaard Peter, SorensenBoe Sandahl, Correlation between circulating mutant DNA and metabolic tumour burden in advanced non-small cell lung cancer patients, Br. J. Cancer 117 (2017) 704–709.

[34] E. Huynh, T. Coroller, V. Narayan, V. Agrawal, Y. Hou, J. Romano, I. Franco, R. Mak, H. Aerts, CT-based radiomic analysis of stereotactic body radiation therapy patients with lung cancer, Radiother. Oncol. 120 (2016) 258–266.

[35] T. Coroller, V. Agrawal, V. Narayan, Y. Hou, P. Grossmann, S. Lee, R. Mak, H. Aerts, Radiomic phenotype features predict pathological response in non-small cell lung cancer, Radiother. Oncol. 119 (2016) 480–486.

[36] H. Kim, C. Park, J. Goo, J. Wildberger, H. Kauczor, Quantitative computed tomography imaging biomarkers in the diagnosis and management of lung cancer, Invest. Radiol. 50 (2015) 571–583.

[37] E. Cernadas, D. Amorim, Do we need hundreds of classifiers to solve real world classification problems? J. Mach. Learn. Res. 15 (2014) 3133–3181.